Physica 23D (1986) 155–168
North-Holland, Amsterdam

ELECTRONIC AND ELASTIC MODE LOCKING IN CHARGE DENSITY WAVE CONDUCTORS

A. ZETTL
Department of Physics, University of California, Berkeley, CA 94720, USA

Mode locking phenomena are investigated in the charge density wave (CDW) materials $NbSe_3$ and TaS_3. The joint application of ac and dc electric fields results in free running and mode locked solutions for the CDW drift velocity, with associated ac-induced dynamic coherence lengths $\xi_D(ac)$ on the order of several hundred microns. The electronic response couples directly to the elastic properties of the crystal, with corresponding free running and mode locked solutions for the velocity of sound. Phase slip center-induced discontinuities in the CDW phase velocity lead to mode locked solutions with period doubling routes to chaos, and noisy precursor effects at bifurcation points. These results are discussed in terms of simple models of CDW domain synchronization, and internal CDW dynamics.

1. Introduction

In a growing number of low dimensional conductors, there exists, below a transition temperature ranging from 50 K to 300 K, a charge density wave (CDW) ground state with associated excitation energies on the order of millikelvin (measured on a per electron basis) [1]. Stability against thermal fluctuations is provided by the large number of carriers condensed in the collective CDW state, and to first order a zero temperature formulation of the dynamics is appropriate. The static CDW may exhibit phase coherence over macroscopic distances determined by the (impurity dependent) Lee–Rice length [2]. Static coherence lengths ξ_s are on the order of fractions of microns for pure specimens of $NbSe_3$ and TaS_3, with comparable lengths expected for $(TaSe_4)_2I$ and $K_{0.3}MoO_3$.

In the presence of relatively low (mV/cm) applied dc electric fields exceeding a threshold field E_T, the CDW condensate may depin from the underlying lattice, thereby carrying a real electric current [3, 4]. CDW conductors are thus intrinsic nonlinear devices. The depinned current driven CDW generates incoherent and coherent voltage oscillations across the ends of the specimen [4], and most likely also throughout the bulk of the crystal [5]. The coherent oscillations ("narrow band noise") have a fundamental frequency directly proportional to CDW current, and hence proportional to CDW drift velocity [6].

Quite analogous to what is observed in Josephson junctions or superconducting microbridges [7], in CDW systems the joint application of dc and ac electric drive fields leads to "interference" in the electronic response [6]. In particular, the CDW phase velocity may mode lock to the frequency of the ac drive field, resulting in "Shapiro steps" in the dc current voltage characteristics [8, 9].

In this report we investigate the fine structure of such mode locking, and its implications for CDW coherence. We also investigate the effect of electronic mode locking on the macroscopic elastic properties of the CDW crystal. Finally, we examine the effects of intentional "breaking" of the macroscopic CDW phase coherence, in particular the consequent transitions to chaos.

2. Electronic mode locking

2.1. *Domains and synchronization*

The joint application of dc and ac electric fields (or currents) to CDW conductors results in sharp

0167-2789/86/$03.50

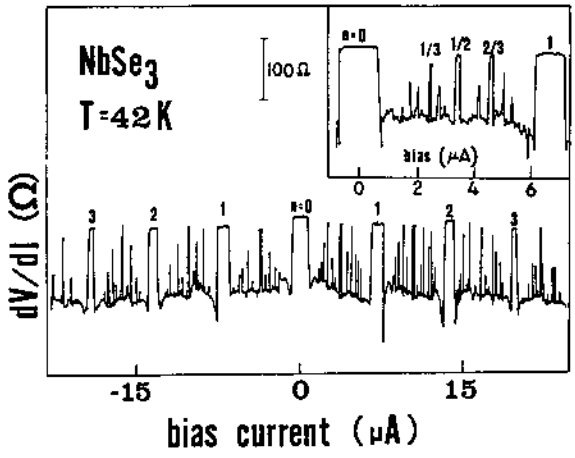

Fig. 1. Shapiro step spectrum in $NbSe_3$. The mode locked steps are indexed by $n = \omega_N/\omega_{ex}$. The inset shows in detail the subharmonic structure, with non-integral $n = p/q$. $\omega_{ex}/2\pi = 5$ MHz.

Shapiro step interference. Fig. 1 shows the effect for $NbSe_3$ at 45 K. The excitation applied to the sample is a current of the form $I = I_{dc} + I_{ac}\cos(\omega_{ex}t)$. At $I_{dc} = 0$, the (dc) differential resistance dV/dI is finite, and corresponds strictly to the normal electron resistance, assumed to be in parallel with the CDW condensate. For finite I_{dc}, a spectacular array of interference peaks is observed. These occur whenever the narrow band noise frequency, ω_N, equals $n\omega_{ex}$, with $n = p/q$ where p and q are positive integers [10]. Integral n corresponds to "harmonic" Shapiro steps, while nonintegral n corresponds to "subharmonic" steps. Subharmonic structure is shown in detail in the inset to fig. 1.

An important feature of the harmonic (and some subharmonic) interference peaks of fig. 1 is that their tops are flat, i.e. over a finite range in I_{dc} (corresponding to a finite range in applied dc field E_{dc}), dV/dI is constant. Over this range the CDW is *mode locked* to ω_{ex}, and changes in E_{dc} have no effect on v_d, the CDW drift velocity. If, on a particular step, the *entire* CDW condensate were mode locked, then dV/dI on that step would attain *exactly* $dV/dI(I_{dc} = 0)$. Such "complete" mode locking is, however, not observed in fig. 1 (although the locking there is very nearly complete). The actual height h of the interference peak, measured from the effective baseline (or saturated dV/dI value) represents the volume fraction of the CDW condensate mode locked to the external ac drive. This is simply understood if we consider the CDW conductor as a series of CDW "domains", as depicted in fig. 2. Each domain there consists of a charged CDW "particle" in a periodic pinning potential, in parallel with a resistance R_n representing normal electrons. Differences in CDW phase velocity from one domain to the next are compensated by carrier conversion at vertical resistor junctions. The CDW particle associated with each domain has a differential resistance R_{CDW}, where $R_{CDW} \to \infty$ if the domain is mode locked, and $R_{CDW} \to R_c$ (a constant) in the conduction saturated (unlocked) limit. In this model, the total differential resistance for the sample is

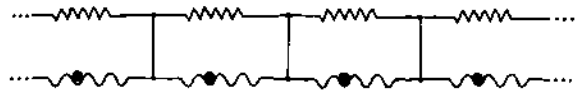

Fig. 2. Domain model for CDW conductor. The resistors represent normal electrons in parallel with charged CDW "particles" in periodic potentials. Carrier conversion is allowed by vertical shunts.

$$dV/dI = \sum_{j=1}^{N} R_n R_{CDW}/(R_n + R_{CDW}), \qquad (1)$$

where j indexes the domain and N is the total number of domains in the crystal. If all N domains are mode locked, $dV/dI = \sum_{j=1}^{N} R_n = dV/dI(I_{dc} = 0)$, and $h = h_{max} = \sum_{j=1}^{N} R_n - \sum_{j=1}^{N} R_n R_c/(R_n + R_c)$. If, on the other hand, only M of the N domains are mode locked,

$$h = \sum_{j=1}^{M} R_n + \sum_{j=M+1}^{N} R_n R_c/(R_n + R_c) - \sum_{j=1}^{N} R_n R_c/(R_n + R_c).$$

This implies $h/h_{max} = M/N$, the locked volume fraction.

Experimentally, for a given Shapiro step (indexed by n), the ratio h/h_{max} depends on both the ac electric field amplitude E_{ac} and frequency ω_{ex}. In general, higher $E_{ac}(E_{ac} \geq 3E_T)$ and lower ω_{ex} (low MHz range) leads to more complete mode locking. The size of the CDW crystal also plays an important role, with "typical" $NbSe_3$ and TaS_3 crystals of dimensions 1 μm × 10 μm × 1 mm (chain axis) rarely displaying complete mode lock. This suggests that the *ac-induced* CDW phase velocity coherence length ξ_D(ac) is less than 1 mm.

To determine ξ_D(ac) explicitly, one may explore mode locking for a single crystal over different spatial ranges. Fig. 3 shows the results for such an experiment in $NbSe_3$, where non-perturbative "sliding" voltage sensing probes were used to determine h/h_{max} for the $n = 1$ Shapiro step, as a function of distance d between voltage probes. For $d > 500$ μm, h/h_{max} decreases with increasing probe separation, while $h/h_{max} = 1$ for $d < 500$ μm. This determines ξ_D(ac) ≈ 500 μm for relatively pure specimens of $NbSe_3$. Within a length on the order of 500 μm, all domains may be fully mode locked by the external ac electric field.

Fig. 4 is an example of complete CDW mode locking in $NbSe_3$, at least for the $n = 1$ and $n = \frac{1}{2}$ Shapiro steps. The sample used for this study had a total length 200 μm ($< \xi_D$(ac)). Fig. 4 shows

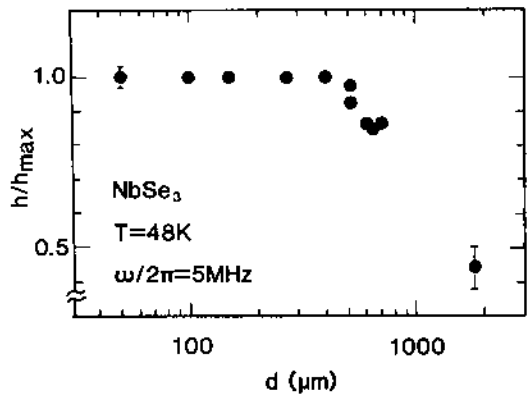

Fig. 3. Degree of mode lock h/h_{max} for a single $NbSe_3$ crystal, as a function of distance d between voltage sensing probes. For $d \leq 500$ μm = ξ_D(ac), complete mode locking is achieved.

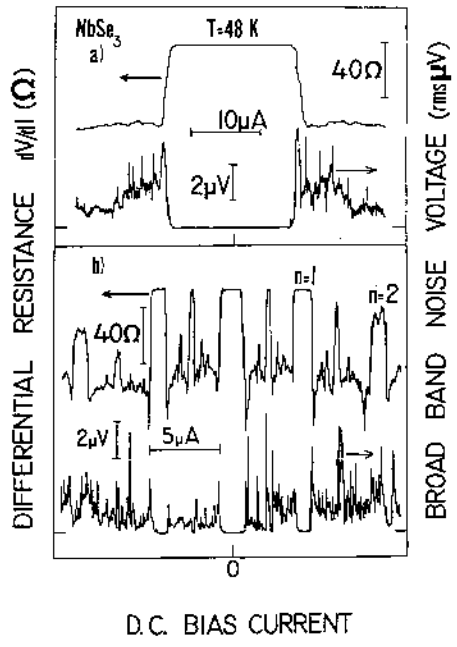

Fig. 4. dV/dI and broad band noise amplitude in $NbSe_3$, as functions of dc bias. a) No ac field present; b) with an applied ac field at $\omega_{ex}/2\pi = 2$ MHz. The broad band noise vanishes on mode locked steps.

another important feature associated with complete mode locking, that of broad band noise suppression [11]. In the absence of ac drive field, a depinned CDW generates $1/f$ "broad band" noise in addition to the narrow band noise [4, 12]. The broad band noise amplitude for $NbSe_3$ is shown in fig. 4a as a function of I_{dc}. Fig. 4b shows clearly that, for joint ac and dc applied fields, the broad band noise amplitude vanishes identically on completely mode locked Shapiro steps. On steps for which $h/h_{max} < 1$, the noise amplitude is significantly reduced, but still finite. This suggests that the broad band noise is a consequence of phase velocity fluctuations arising from unlocked domains, and is thus in many ways analogous to $1/f$ noise in metal due to resistance fluctuations [13]. Broad band noise in TaS_3 has been investigated in some detail by Bhattacharya et al. [14], in terms of local fluctuations in E_T and domain structure.

In fig. 2, the dynamics of each domain might be described to first order by a "rigid particle" equation of motion, such as that introduced by Grüner,

Zawadowski and Chaikin [15],

$$d^2x/dt^2 + (\tau_{CDW}^{-1})\,dx/dt + \omega_0^2 \sin(Qx)/Q = eE/m^*, \quad (2)$$

where x is the CDW position, τ_{CDW} is a phenomenological CDW relaxation time, ω_0 is the CDW resonance frequency, $Q = 2\pi/\lambda$ with λ the CDW wavelength, m^* is the effective CDW electron mass, and $E = E_{dc} + E_{ac}\cos(\omega_{ex}t)$. Eq. (2) in itself predicts narrow band noise and mode locking, but no broad band noise (with exception to chaotic response to be discussed later). The dynamics of the entire CDW condensate then depends on how domains interact. The important feature demonstrated by the experiments just described is that the external ac field serves to couple domains together, i.e. synchronize them. The "synchronization length" is ξ_D(ac), and is a direct measure of ac field induced phase homogenization. With $E_{ac} \to 0$, some synchronization is still possible, due to self-synchronization. This may account for the sharp frequency structure of the narrow band noise in the presence of E_{dc} alone. The self-synchronization length is $\xi_D < \xi_D$(ac), and has been estimated from narrow band noise studies to be on the order of 0.5 μm [16].

Synchronization and self-synchronization are often found in biological systems [17] (e.g. circadian rhythm) or laser physics [18], where complete (and partial) mode locking are commonplace. A single domain in such systems is often described by the van der Pol equation [19], which, for small displacements, differs from eq. (2) only in the form of the dissipative coefficient, which introduces nonlinear feedback. For linearly coupled van der Pol oscillators, subgroups of the entire oscillator set may mode lock, analogous to incomplete mode locking displayed in fig. 1. A linear interaction between oscillators in CDW systems could be easily mediated through frictional forces or ohmic currents. It should also be noted that sets of coupled oscillators, where each oscillator is described by eq. (2), display similar synchronization properties, as demonstrated by dynamics of Josephson junction arrays [20].

2.2. *Harmonic and subharmonic structure*

The simplest analysis of Shapiro steps in CDW systems results when CDW internal degrees of freedom are neglected, and one assumes only a single coordinate for the CDW phase, for example eq. (2). In dimensionless form, eq. (2) reads

$$d^2\theta/dt^2 + G\,d\theta/dt + \sin\theta = E/E_T, \quad (3)$$

where $G = (\omega_0\tau_{CDW})^{-1}$ and time is measured in units of ω_0^{-1}. This equation is well known in the Josephson junction literature [7], where it describes the phase difference between superconductors comprising a resistively shunted junction (with E/E_T replaced by I/I_T, and G related to junction resistance, capacitance, and plasma frequency by $G = (RC\omega_J)^{-1}$). Eq. (3) predicts Shapiro step interference and mode locking, and, in the overdamped limit, it provides surprisingly good quantitative fits to the behavior of the $n = 1$ mode locked step in $NbSe_3$ over a wide range of ac drive frequency and amplitude [8]. The return map appropriate to eq. (3) is a *one*-dimensional sine circle map [21],

$$\theta_{m+1} = \theta_m + \Omega + K\sin(2\pi\theta_m)/2\pi, \quad (4)$$

where m is a discrete time index, i.e. the system is stroboscopically viewed at discrete times $t_m = 2\pi m/\omega_{ex}$, $\Omega = \omega_N/\omega_{ex}$, and K represents the strength of the coupling of the system to the external drive. For the CDW system, we associate K with E_{ac}. The circle map describes in a natural way the interaction of resonances, and indeed harmonic and subharmonic mode locked solutions follow directly from eq. (4) [21]. The mode locked steps are separated by regions of quasiperiodic orbits; these "gaps" comprise less and less of Ω space as K increases from zero and approaches a critical line at $K = 1$. For $K < 1$, the mode locked steps form an (incomplete) devil's staircase of dimension $d = 1$. At $K = 1$, the staircase is complete, with a fractal dimension $d = 0.870$. This is the Hausdorff dimension of the complementary Cantor set for the mode locked region. For $K > 1$,

resonances overlap and the map is no longer invertible, and chaos is possible. The fractal dimension $d = 0.87$ near criticality is not restricted to the sine circle map, but holds for a wide class of return maps [22].

To test for completeness of the devil's staircase, one could count up the widths of all mode locked regions in Ω space, and determine if the quasiperiodic orbits (gaps) are confined to a Cantor set of zero measure. A more practical (finite resolution) method is to consider the gaps themselves. Given a scale r, the total measure of the gaps between mode locked steps is $1 - S(r)$, and the number of holes $N(r) = [1 - S(r)]/r$. If $rN(r) \to 0$ as $r \to 0$, the staircase is complete, with fractal dimension d given by [21]

$$N(r) \propto r^{-d}. \tag{5}$$

An analysis such as that just described by Brown et al. [23] on Shapiro step interference in $NbSe_3$ has indicated a fractal dimension $d = 0.91$, with no apparent dependence on E_{ac}. Unfortunately, in that experiment no complete mode locking was observed, and hence the interference peaks (and thus also gaps) were of ill-defined width. Fig. 5 shows an analysis of subharmonic mode locked steps in a high quality $NbSe_3$ sample (where locking was virtually complete), for four different values of V_{ac} ($V_{ac} = I_{ac}R_0$, with R_0 the ohmic sample resistance). For all four cases the data points of $\log N(r)$ vs $\log(1/r)$ fall excellently on a straight line, consistent with the expected power law behavior of eq. (5). The inset to fig. 5 shows the V_{ac} dependence of d. Although the fractal dimension corresponding to $V_{ac} = 330$ mV is 0.862, and hence very close to the value 0.870 expected from the circle map at $K = 1$, d in fig. 5 is observed to increase with increasing ac drive amplitude, and appears to asymptotically approach $d = 1$ at high V_{ac}.

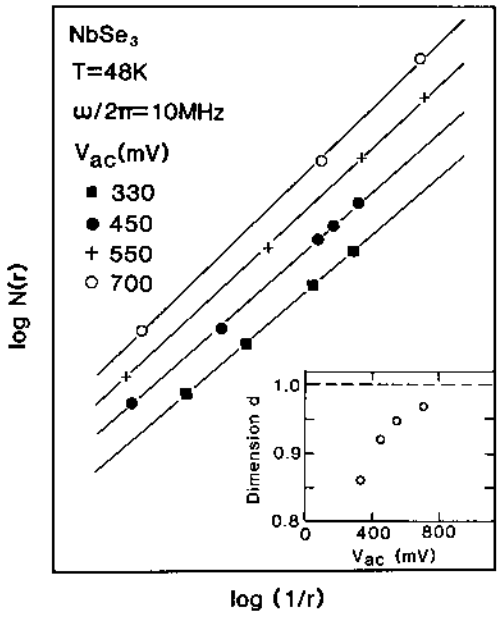

Fig. 5. $\log N(r)$ vs $\log(1/r)$ for Shapiro step subharmonic structure in $NbSe_3$. The traces corresponding to different V_{ac} have been offset for clarity. The inset shows the resulting fractal dimension d vs ac amplitude. At high V_{ac}, d tends toward 1.0.

Similar results follow from an analysis of subharmonic mode locked steps if d is determined from a Farey tree construction [24], where

$$\sum_i (s_i/\tilde{s})^d = 1. \tag{6}$$

s_i and $\tilde{s}$ are defined as follows: Starting with any pair of locked intervals p/q and p'/q', the length between them is denoted $\tilde{s}$. Next the locked interval $(p + p')/(q + q')$ is determined, yielding gaps of length s_{i-1} and s_{i-2} between the new interval and the preceding one. The process is then repeated until the experimental (or numerical) resolution is exhausted. Surprisingly, this method appears to give d to within a few percent accuracy using only two gaps. Applying this method to $NbSe_3$, d is found [25] to increase with increasing V_{ac}, approaching $d = 1$ at high ac drive field, consistent with the data of fig. 5.

The V_{ac} dependence of the dimension d observed in $NbSe_3$ is inconsistent with the predictions of the circle map, where $d = 1$ at low ac

drive, and $d = 0.870$ only at (or very close to) the critical line. In addition, for the types of $NbSe_3$ samples here discussed (non-switching, see section 4) there is no transition to chaos for large ac drive, again in contrast to what might be expected from the circle map. An interpretation of the mode locking structure in CDW systems in terms of the circle map (or eq. (3)) has other serious problems, the most apparent being that subharmonic structure is not predicted unless the inertial term of eq. (3) is retained. This is, however, not consistent with low field ac conductivity studies, which indicate an overdamped (noninertial) response [9]. This problem can of course be overcome if a non-sinusoidal potential is introduced into eq. (3) [26].

A more realistic approach to the Shapiro step interference includes CDW internal degrees of freedom. A full hydrodynamical solution to the CDW problem by Sneddon, Cross, and Fisher [27] leads to ac-induced interference structure in the $I-V$ characteristics, but no true mode locking. The CDW condensate has also been treated as a series of masses connected by springs in a pinning potential [28], and for this model Coppersmith [29] finds harmonic and subharmonic mode locking. Here the internal CDW degrees of freedom (provided by the springs) play a key role in the subharmonic structure. Short range deformations of the CDW have also been considered by Tua and Ruvalds [30], who numerically solve a classical equation of motion assuming a large number of interacting CDW segments. A devil's staircase structure is obtained, although there appears to be no power law behavior consistent with eq. (5), and hence no fractal dimension can be inferred. More consistent with the domain structure described earlier (fig. 2), Doniac and coworkers [31] have treated the CDW as two coupled (overdamped) oscillators, each independently obeying eq. (3). Sharp subharmonic structure is indeed found. It remains to be seen if such a model, extended to more than two domains, can account for incomplete mode locking or devil's staircase behavior with fractal dimension.

It is nevertheless clear that internal CDW dynamics play an important role in the fine structure of CDW mode locking, and that a single degree of freedom model, such as eq. (3), is inadequate, in particular in describing quasiperiodic orbits where broad band noise abounds.

3. Elastic mode locking

3.1. *Coupling of electronic–elastic response*

The electronic mode locking phenomenon discussed in section 2 reflects directly the free running or locked solutions of θ, and hence also solution of the CDW drift velocity $v_d \propto \langle d\theta/dt \rangle$. This suggests that other CDW properties, sensitive to v_d, should be affected by electronic mode locking. One such property, the broad band noise amplitude, has already been discussed. Experiments on $TaSe_3$ by Brill and Roark [32], and other CDW materials by Mozurkewich et al. [33], have shown that the bulk elastic properties of CDW crystals are sensitive to CDW motion. In TaS_3, for example, the Young's modulus Y decreases with increasing $E_{dc} > E_T$, and eventually saturates. Similarly, the internal friction δ increases with increasing $E_{dc} > E_T$, and also saturates (in fact much more quickly than does Y). A simple interpretation of these results is that in the pinned state, the stiffness of the CDW adds to that of the lattice, while a depinned CDW is decoupled from the lattice, and hence the stiffness of the lattice is reduced. Such arguments lead to order of magnitude estimates [33] in changes of Y upon depinning, which are in rough agreement with experiment.

In the region of ac-induced electronic mode locking, where v_d is fixed over a finite range in E_{dc}, one might expect Y and δ to display no more than "regions of constancy" during mode locking. This would occur if Y and δ were strictly functions of v_d. Alternatively, one might imagine that during mode locking, the CDW would fully decouple from the underlying lattice. In this case, Y

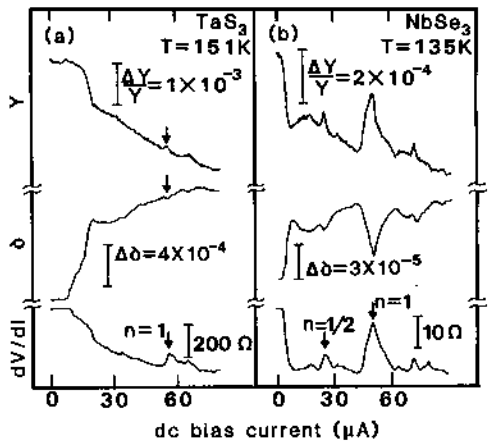

Fig. 6. Young's modulus, internal friction δ, and dV/dI in TaS_3 and $NbSe_3$. Shapiro step electronic interference results in corresponding anomalies in Y and δ. Vertical arrows identify interference structure in TaS_3.

and δ would, during electronic mode locking, assume their high field, saturated values.

Fig. 6 shows that an entirely different behavior is observed for Y and δ during mode locking in TaS_3 and $NbSe_3$. During the Shapiro step interference, Y and d both tend toward their *zero* field, pinned values. This occurs for harmonic as well as subharmonic electronic mode locking. The effect is more dramatic for $NbSe_3$ (fig. 6b), for which the electronic locking is approximately 75% complete for the $n = 1$ interference step. For both TaS_3 and $NbSe_3$, a rough scaling exists between the degree of electronic mode lock (i.e. h/h_{max}) and the size of the anomaly in Y and δ during mode lock. During complete mode lock, it is thus expected that Y and δ achieve exactly their zero bias values. We term the anomalies in Y and δ elastic mode locking, since here the velocity of sound is locked to a value dictated only by $(d/dt)[\langle d\theta/dt\rangle]$, assuming complete electronic mode locking. Experiments performed on samples which display complete electronic mode locking would no doubt reveal Y or δ vs E_{dc} structure quite analogous to the devil's staircase for the electronic interference, presumably with an identical fractal dimension. The difficulty in performing such experiments lies in the fact that $\xi_D(ac)$ is on the order of several hundred microns (see fig. 3), a rather restrictive length for elastic measurements.

3.2. *Role of internal degrees of freedom*

To describe elastic effects in CDW conductors, one must clearly include the compressibility of the lattice, if not that of the CDW as well. Simple "rigid particle" models, such as eq. (2), are entirely inadequate to describe elastic response. Coppersmith and Varma [34] have proposed a model where a rigid CDW interacts with a deformable lattice. Although an anisotropy is obtained in the velocity of sound for a moving CDW, the effect is orders of magnitude smaller than the observed changes in Y and δ due to CDW depinning in $NbSe_3$ and TaS_3. This suggests that the changes in Y and δ are also linked to internal degrees of freedom of the CDW condensate. The behavior of Y and δ in dc fields alone has been examined by Brill [35] in terms of an anelastic relaxation model. When a distortion occurs, the system is driven far from equilibrium, and the relaxation back is associated with a characteristic time constant τ. If $\tau = \tau(E_{dc} - E_T)$ and is long compared to the period of the elastic distortion (i.e. the elastic resonance frequency), Y and δ will change with increasing $E_{dc} > E_T$. The shapes of the functions $Y(E_{dc})$ and $\delta(E_{dc})$ can be reproduced qualitatively by such a model, but their relative magnitudes cannot. τ may be associated with the relaxation of sliding domain walls [32, 35]. The electronic studies of mode locking described in section 2 indicate that CDW phase coherence is enhanced dramatically during mode locking. In terms of a domain wall relaxation model, mode locking then either eliminates domain walls entirely, or drastically shortens their relaxation time.

Elastic mode locking has been explicitly considered by Sherwin and Zettl [36] in a simple many degree of freedom model which takes into account interactions between the deformable CDW and modes of the underlying lattice. The equations of motion, derived from a discretized sine-

Gordon model with discretized lattice mass units, are

$$m\,\mathrm{d}^2 r_j/\mathrm{d}t^2 + \gamma\,\mathrm{d}(r_j - x_j)/\mathrm{d}t + k(2r_j - r_{j+1} - r_j) + QV\sin\left[Q(r_j - x_j)\right] = f_j(t), \quad (7)$$

$$M\,\mathrm{d}^2 x_j/\mathrm{d}t^2 + \Gamma\,\mathrm{d}(2x_j - x_{j+1} - x_{j-1})/\mathrm{d}t + \gamma\,\mathrm{d}(x_j - r_j)/\mathrm{d}t + K(2x_j - x_{j+1} - x_{j-1}) + QV\sin\left[Q(x_j - r_j)\right] = F_j(t), \quad (8)$$

where r_j and x_j are respectively the (laboratory frame) positions of the jth CDW mass and jth lattice unit. γ represents damping of the CDW particles, $Q = 2\pi/\lambda$ with λ the CDW wavelength, V is the strength of the impurity pinning force, and Γ represents internal friction of the lattice. f_j represents the external force on the CDW (provided by the external electric field), and F_j is the mechanical force applied to the lattice, the response to which determines Y and δ. Eqs. (7) and (8) describe an infinite set of coupled equations. A reduced form of these equations has been solved in the limit of combined ac and dc drive electric fields to the CDW [36]. It is found that Shapiro step mode locking in the electronic response (also predicted by eqs. (7) and (8)) is indeed associated with mode locked solutions of Y and δ, in striking agreement with the behavior observed in fig. 6. Hence, the mode locking of the elastic response follows directly from a simple model where CDW internal degrees of freedom are taken into account. A model similar to Eqs. (7) and (8) has been independently proposed by Sneddon [37], but solved only in the limit of finite E_{dc}, with $E_{ac} = 0$.

4. Breaking of the CDW coherence and transitions to chaos

The long range phase coherence induced in CDW conductors by the application of ac and dc electric fields may be destroyed by a number of mechanisms, for example strong impurities, or non-uniform threshold fields arising from non-uniform temperature distributions in the crystal. Under such conditions there may result in a single crystal several macroscopic regions, each fully and independently phase velocity coherent. The interfaces between regions can be surprisingly sharp, and the dynamics of such crystals may be dramatically different from those associated with "unstressed" specimens previously described.

4.1. *Effects of a temperature gradient*

Although it was argued earlier that temperature may not play an important role in describing excitations of the CDW condensate, most CDW transport properties are quite temperature dependent. For example, in $NbSe_3$ and TaS_3, E_T tends to increase at low temperatures, and diverge as the CDW temperature is approached from below. The ratio I_{CDW}/ω_N is also temperature dependent, and reflects the number of carriers condensed in the CDW state [9]. I_{CDW} is the current carried by the condensate. In general, then, the function $\omega_N(I_{dc})$, with ω_N the intrinsic "washboard" frequency for each domain (or local narrow band noise frequency) is temperature dependent. The synchronization and self-synchronization effects discussed previously, and indeed the determination of $\xi_D(ac)$ itself, assumed isothermal conditions for the CDW crystal. In the presence of an applied temperature gradient, each CDW domain (see fig. 2) might be associated with an independent R, E_T, and $\omega_N(I_{dc})$ [38]. An important question is thus if macroscopic synchronization, and hence macroscopic phase velocity coherence, can be retained in the presence of a temperature gradient.

Fig. 7 shows the effect of a uniform temperature gradient on electronic mode locking in $NbSe_3$. ΔT represents the total temperature difference across the sample, with the (cold) end of the sample fixed at $T_0 = 47$ K. With zero gradient, this high quality crystal displays complete mode lock for the $n = 1$ step, and several subharmonic steps as well. With increasing ΔT, the Shapiro step spectrum breaks up. For $\Delta T = 2.8$ K, for example, the $n = 1$ "step"

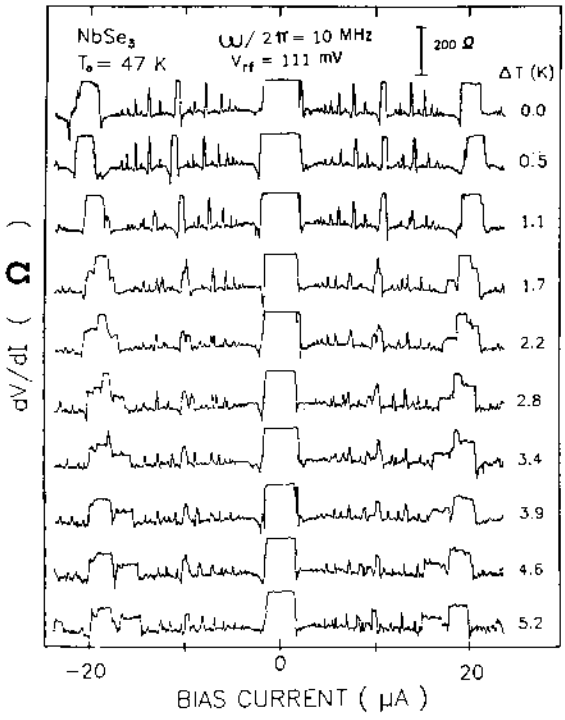

Fig. 7. Shapiro step spectrum of $NbSe_3$ for various values of temperature differential ΔT applied across the length of the crystal. The $n = 1$ step is, for $\Delta T = 0$, located at 20 μA dc bias. Increasing ΔT results in a break-up of the crystal into two distinct macroscopic domains.

has three distinct plateaus; the first (at lowest I_{dc}) has $h/h_{max} = 0.40$, the second has $h/h_{max} = 1.0$, and the third has $h/h_{max} = 0.60$. Since in this temperature range in $NbSe_3$ $\omega_N(I_{dc})$ increases with increasing temperature [9], the first plateau corresponds to mode locking of a "hot" *macroscopic* domain (corresponding to a synchronization of many of the domains as shown in fig. 2). The size of this domain is $\chi_h = 0.40\chi$, where χ is the total sample volume. Similarly, the plateau corresponds to mode locking of a "cold" macroscopic domain, of size $\chi_c = 0.60\chi$. We note that $\chi_c + \chi_h = \chi$, indicating that the hot and cold domain volumes do not intersect. The middle plateau (with $h/h_{max} = 1$) corresponds to the hot and cold domains synchronized together, and hence for these values of V_{ac} and ΔT complete mode lock is still possible for some value of I_{dc}. However, for

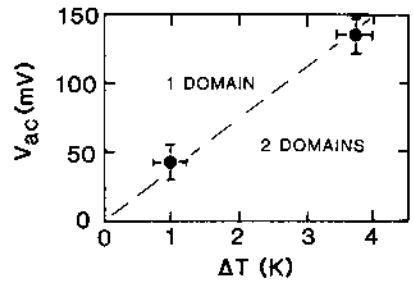

Fig. 8. Critical temperature differential ΔT as a function of V_{ac}, for which a $NbSe_3$ crystal breaks from a single, macroscopically coherent domain, to two independently coherent macroscopic domains. $\omega_{ex}/2\pi = 10$ MHz.

the trace corresponding to $\Delta T = 3.9$ K in fig. 6, this is no longer the case; there the hot and cold macroscopic domains mode lock independently to ω_{ex} (for different values of I_{dc}), but never synchronize to one another. This defines a critical ΔT above which complete mode locking is no longer possible for the entire crystal (but is still possible for each of two independent macroscopic domains of smaller volume). On the other hand, even for ΔT exceeding this critical temperature, the hot and cold domains *can* be forced to again synchronize, by applying a sufficiently strong ac field [39]. Hence ΔT (critical) is V_{ac} dependent.

Fig. 8 shows the critical ΔT needed to fully "break" CDW coherence, as a function of V_{ac} in $NbSe_3$. This figure essentially determines the maximum $\xi_D(ac)$ as a function of ΔT and V_{ac}: in the 1-domain region $\xi_D(ac)_{max} = 500$ μm, the total sample length, while in the 2-domain region $\xi_D(ac)_{max} = 0.6(500\ \mu m) = 300\ \mu m$, the size of the cold domain. An interesting question is if more than two macroscopic domains can form, for example for very large values of ΔT. Most probably this is the case, as can be inferred from narrow band noise measurements on $NbSe_3$, which have shown three or more independent noise peaks in the presence of large temperature gradients [40].

4.2. *Switching and phase slip centers*

Switching refers to sharp jumps in the I–V characteristics of CDW conductors; it occurs for

both voltage driven and current driven situations. Often switching occurs at E_T, and it then corresponds to the onset of CDW conduction [41]. Although switching is observed in "nominally pure" materials, it can be induced by chemical doping or irradiation [42], and hence appears to be a (temperature dependent) strong impurity effect. Crystals which display switching also display transport properties quite different from those associated with those of nonswitching crystals (of the same material). For example, in $NbSe_3$ switching is associated with hysteresis [41], negative differential resistance [43], bistability and strong $1/f$ noise [43], inductive ac response [44], multiple sublevel states [45], and chaos [46]. All these effects are absent in nonswitching samples of $NbSe_3$.

Recent experiments [47] have demonstrated that switching is associated with a break-up of the CDW condensate into macroscopic regions with independent threshold fields E_T and independent CDW phase velocities. The interface between these regions corresponds to spatially localized phase slip centers, where the CDW amplitude undergoes successive fluctuations and across which CDW phase coherence is broken. It appears that the CDW dynamics at the phase slip centers themselves may play an important role in the overall dynamics of the CDW condensate.

In the presence of combined ac and dc electric fields, complete mode locking may occur in the switching regime of $NbSe_3$, as demonstrated in fig. 9. In this I–V representation, the Shapiro steps are the (relatively wide) "horizontal" steps; the sharper vertical steps represent transitions to higher order (harmonic) steps. In switching samples, the harmonically locked regions thus fill up practically all of Ω space, in contrast to the large gaps between harmonically mode locked regions observed in the non-switching crystal of fig. 1. Although not apparent from fig. 9, between the mode locked harmonic steps there exist subharmonic steps. This structure may be analyzed using the methods outlined in section 2.2. Fig. 10 shows the fractal dimension d as a function of V_{ac} for a switching sample of $NbSe_3$, determined from

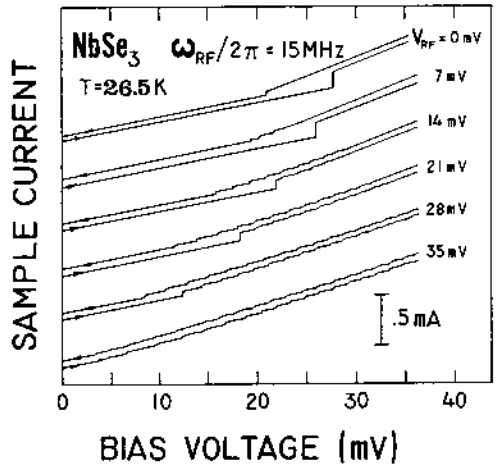

Fig. 9. Shapiro steps in switching regime of $NbSe_3$. The sample is voltage driven; the Shapiro steps are the wide "horizontal" steps which appear for $V_{rf} \geq 7$ mV. The traces for forward and reverse bias sweep have been offset vertically for clarity.

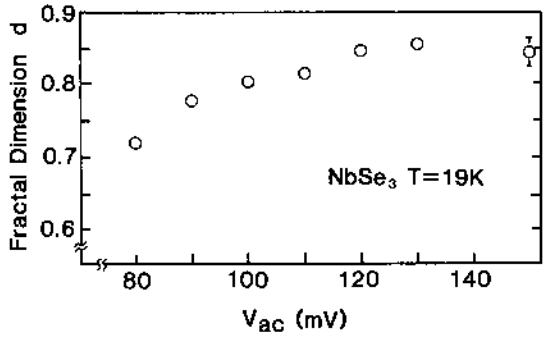

Fig. 10. Fractal dimension d for subharmonic Shapiro step structure of $NbSe_3$ in switching regime. At high values of V_{ac}, d tends toward $d \simeq 0.85$.

eq. (6) using the first two gaps. Quite analogous to the behavior of fig. 5, d increases with increasing V_{ac}, and appears to saturate at high V_{ac}. In contrast to fig. 5, however, here, for the switching crystal, the limiting value of d appears to be $d = 0.85$, rather than 1.0. This difference may have relevance to the chaotic response of $NbSe_3$, observed only in the switching regime.

4.3. *Chaotic response and noisy precursors*

As discussed previously, on mode locked Shapiro steps the CDW drift velocity becomes

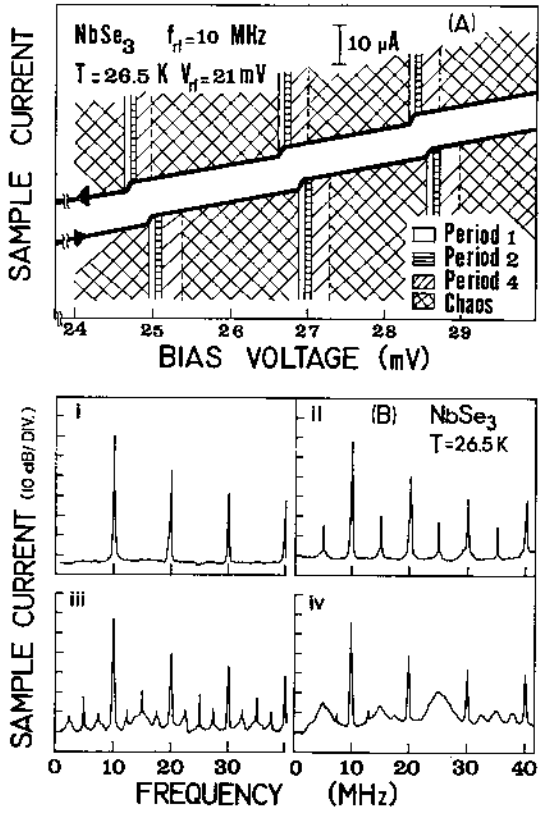

Fig. 11. a) $I-V$ characteristics and associated frequency response for $NbSe_3$ in switching regime. On each mode locked step, a period doubling route to chaos is observed. b) Frequency response spectra corresponding to (i) period 1; (ii) period 2; (iii) period 4; (iv) chaos.

locked to the external ac drive frequency ω_{ex}. In addition, phase velocity fluctuations are suppressed, as evidenced by the absence of broad band noise on mode locked Shapiro steps. In the switching regime, there exist on the mode locked steps well defined transitions to chaos. Fig. 11a shows schematically the dc and ac response of switching $NbSe_3$ on mode locked steps. The heavy lines represent the dc $I-V$ characteristics for forward and reverse bias sweep; the vertical "windows" represent the nature of the ac response for that particular range of dc bias voltage. Note that this is a voltage driven experiment. At the start of each Shapiro step, the response is periodic with period one. Increasing V_{dc} leads, on each step, to a period doubling route to chaos. The actual ac response is indicated in fig. 11b for four different values of V_{dc}. The higher harmonics apparent in (i) (period one) result from the nonlinear ac CDW response to a sinusoidal drive.

The chaotic response may be interpreted as an example of universal instability in phase locking for a driven nonlinear system characterized by an intrinsic limit cycle, such as the instabilities associated with the circle map. In the circle map, eq. (5), θ is a modulo 1 variable; thus changing Ω to $\Omega + i$, with i an integer, will not change eq. (5). The pattern of bifurcations to chaos will thus repeat itself as Ω is increased monotonically, consistent with behavior observed in fig. 11a.

The period doubling route to chaos observed on mode locked steps in $NbSe_3$ is in agreement with the predictions of eq. (3), but only for certain values of CDW damping and free oscillation frequency. Essentially what is needed is underdamped motion (similar to the requirement for subharmonic interference), and analysis [46] of the switching, hysteresis, and chaos in $NbSe_3$ leads to values of τ_{CDW}^{-1} and ω_0 orders of magnitude smaller than the corresponding values for $NbSe_3$ determined outside the switching regime. Numerical solutions [48] to eq. (3) also indicate chaos only in a rather restricted frequency range given by $(\omega_0^2\tau_{CDW}^2)^{-1} < \omega_{ex}/\omega_0^2\tau_{CDW} < \omega_0\tau_{CDW}$, although chaotic response in $NbSe_3$ is observed over a much wider frequency range.

In $NbSe_3$ a period doubling route to chaos, such as that induced by sweeping V_{dc}, also occurs if the ac amplitude V_{ac} is increased monotonically. Transitions between periodic and chaotic orbits may also be induced by changes in the external drive frequency ω_{ex}. Fig. 12 shows the type of response generated in $V_{ac}-\omega_{ex}$ parameter space, with associated boundaries between characteristic responses. This portrait is actually a projection of the response in $(V_{dc}, V_{ac}, \omega_{ex})$ space onto the V_{dc} plane. The projected response refers to the "highest order" response, i.e. that corresponding to the closest approach to chaos. For example, in the area of fig. 12 identified as chaos, period one orbits exist for some values of V_{dc}, but for fixed

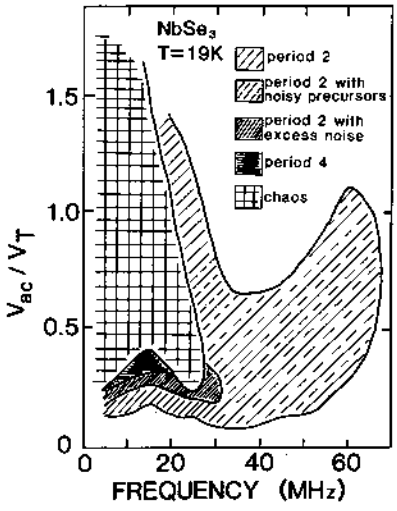

Fig. 12. V_{ac}–ω_{ex} projection of response spectrum in $NbSe_3$ of switching regime. $\omega_{ex}/2\pi = 5$ MHz.

V_{ac} and ω_{ex} chaos is always possible by tuning V_{dc} to an appropriate value. A three dimensional representation of the response in $(V_{dc}, V_{ac}, \omega_{ex})$ space is exceedingly complicated.

Fig. 12 shows regions identified with "excess noise" or "noisy precursors". These regions are of particular interest. Fig. 13 shows an example of the former. Here a single parameter, V_{dc}, was varied smoothly from 151.9 mV to 138.2 mV. The upper trace shows a clear period two solution. As V_{dc} decreases, excess noise appears on the flanks of the $\omega_{ex}/2$ peak. In addition, nearly symmetric frequency structure sets in at $0 + \delta\omega$ and at $\omega_{ex} - \delta\omega$, with $\delta\omega/2\pi = 3$ MHz, apparently unrelated to $\omega_{ex}/2\pi = 20$ MHz. Further decreases in V_{dc} result in a recovery of the pure period two solution, as shown in the bottom trace of fig. 13.

A possibly related phenomenon, that of period two with noisy precursors, is illustrated in fig. 14. Here, ω_{ex} and V_{ac} are again fixed, and V_{dc} is increased smoothly. The top trace shows nearly pure period one behavior, with slight evidence for period two instability. With increasing V_{dc}, symmetric peaks appear, which coalesce into the period two, $\omega_{ex}/2$ peak. With further decreases in V_{dc}, new "sideband" peaks suddenly appear, and move apart with decreasing V_{dc}. The sequence of events

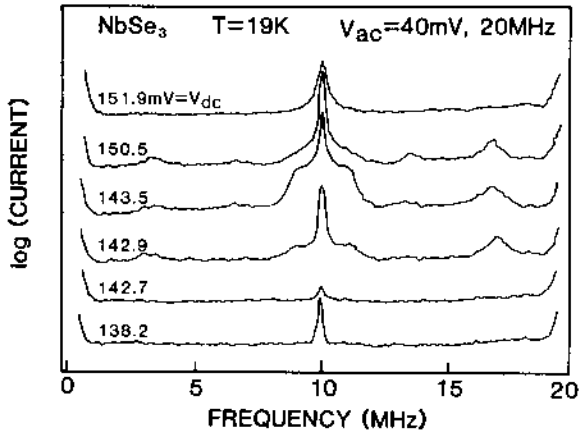

Fig. 13. Current response spectra for $NbSe_3$, corresponding to various values of dc bias. The period 2 response is here associated with excess noise.

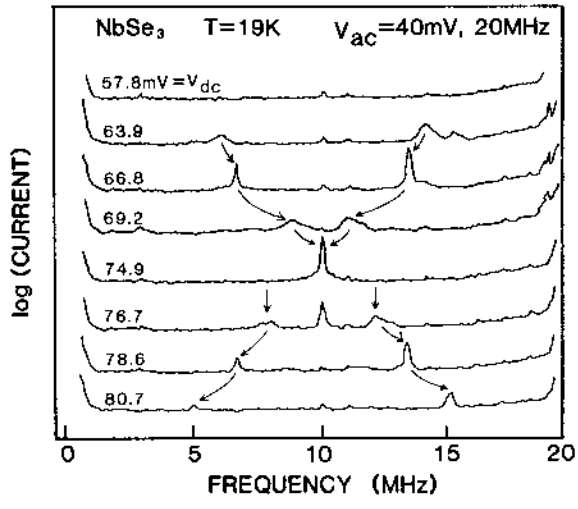

Fig. 14. Current response spectra for $NbSe_3$, corresponding to various values of dc bias. The period 2 bifurcation is here associated with a noisy precursor effect.

in fig. 14 is quite analogous to a noise induced virtual Hopf phenomenon [49], where the noisy precursor of a Hopf bifurcation continuously changes into the precursor characteristic of a period doubling bifurcation. Such virtual Hopf phenomena have been predicted [50] for a Josephson circuit, where the resistive shunt has some inductive character. Similar behavior is in fact predicted by eq. (3), *if* an additional noise term is included [50]. It should be noted that the virtual

Hopf phenomenon is not entirely consistent with the noise-free one dimensional circle map, since the virtual Hopf phenomenon requires a two dimensional mapping.

We thus find that, although the chaotic dynamics observed in $NbSe_3$ in the switching regime can often be accounted for in terms of simple equations of motion or mappings, the details of the response point toward a more complicated dynamics. This is most probably related to velocity-dependent parameters arising from phase slip processes or internal degrees of freedom of the CDW condensate. If models of coupled domains, such as described in section 2, are consistent with the details of the chaotic dynamics, remains to be seen.

5. Conclusion

Charge density wave conductors display a rich spectrum of electronic and elastic mode locking when subjected to combined ac and dc electric drive fields. For unstressed crystals, ac-induced dynamic coherence lengths on the order of several hundred microns can be achieved. This long range coherence is broken by applied temperature gradients, or strong impurity induced phase slip centers which result in switching. Switching crystals further show a wide variety of chaotic response solutions.

The mode locking experiments here discussed show clearly that the CDW condensate cannot in general be described by only a single phase coordinate; intrinsic domain structure and internal degrees of freedom (elasticity) of the CDW play vital roles in the dynamics. It would be desirable to derive models which incorporate such features from a microscopic, rather than phenomenological, basis.

Finally, the ease with which system parameters in CDW materials may be externally manipulated, makes such systems attractive candidates for detailed studies of mode locking phenomena and universal chaotic instabilities.

Acknowledgements

The experiments described in this report were performed by L.C. Bourne, R.P. Hall, M.F. Hundley, and M.S. Sherwin, who are also responsible for many of the ideas expressed. I have benefitted from discussions on mode locking and CDW phenomena with many individuals, in particular S. Coppersmith, P. Bak, M. Jensen, J.W. Brill, P. Littlewood, and G. Grüner. This research was supported by NSF Grant DMR 84-00041. I also gratefully acknowledge support from an IBM Faculty Development Award, and the Alfred P. Sloan Foundation.

References

[1] For a review, see G. Grüner and A. Zettl, Rep. 119 (1985) 117.
[2] P.A. Lee and T.M. Rice, Phys. Rev. B 19 (1979) 3970; H. Fukuyama and P.A. Lee, Phys. Rev. B 17 (1978) 535.
[3] P. Monceau, N.P. Ong, A.M. Portis, A. Meerschaut and J. Rouxel, Phys. Rev. Lett. 37 (1976) 602.
[4] R.M. Fleming and C.C. Grimes, Phys. Rev. Lett. 42 (1979) 1423.
[5] S. Brown and L. Mihaly, Phys. Rev. Lett. 55 (1985) 742.
[6] P. Monceau, J. Richard and M. Renard, Phys. Rev. Lett. 45 (1980) 43.
[7] See, for example, P.E. Lindelof, Rep. Prog. Phys. 44 (1981) 949.
[8] A. Zettl and G. Grüner, Solid State Commun. 46 (1983) 501.
[9] A. Zettl and G. Grüner, Phys. Rev. B 29 (1984) 755.
[10] R.P. Hall and A. Zettl, Phys. Rev. B 30 (1984) 2279.
[11] M.S. Sherwin and A. Zettl, Phys. Rev. B 32 (1985) 5536.
[12] J. Richard, P. Monceau, M. Papoular and M. Renard, J. Phys. C15 (1982) 7157; A. Zettl and G. Grüner, Solid State Commun. 46 (1983) 501.
[13] P. Dutta and P.M. Horn, Rev. Mod. Phys. 53 (1981) 497.
[14] S. Bhattacharya, J.P. Stokes, M.O. Robbins and K.A. Klemm, Phys. Rev. Lett. 54 (1985) 2453.
[15] G. Grüner, A. Zawadowski and P.M. Chaikin, Phys. Rev. Lett. 46 (1981) 511.
[16] G. Mozurkewich and G. Grüner, Phys. Rev. Lett. 51 (1983) 2206.
[17] Y. Aizawa and Y. Kobatake, Prog. Theor. Phys. 53 (1975) 305; A.T. Winfree, J. Theor. Biol. 16 (1967) 15.
[18] M. Sargent III, M.O. Scully and W.E. Lamb Jr., Laser Physics (Addison Wesley, New York, 1974).
[19] Y. Yamaguchi and H. Shimizu, Physica 11D (1984) 212;

Y. Aizawa, Prog. Theor. Phys. 56 (1976) 703.
[20] A.K. Jain, K.K. Likharev, J.E. Lukens and J.E. Sauvageau, unpublished.
[21] M.H. Jensen, T. Bohr, P.V. Christiansen and P. Bak, Brookhaven National Laboratory Report #33495 (1983); M.H. Jensen, P. Bak and T. Bohr, Phys. Rev. A 30 (1984) 1960;
T. Bohr, P. Bak and M.H. Jensen, Phys. Rev. A 30 (1984) 1970.
[22] P. Bak, T. Bohr and M.H. Jensen, Proc. 54th Nobel Symposium, "The Physics of Chaos and Related Phenomena", Gräftaavallen, Sweden, 1984.
[23] S.E. Brown, G. Mozurkewich and G. Grüner, Phys. Rev. Lett. 54 (1984) 2272.
[24] P. Cvitonovic, M.H. Jensen, L.P. Kadanoff and I. Procaccia, unpublished;
I. Procaccia, Physica 8D (1983) 435.
[25] M.S. Sherwin, R.P. Hall and A. Zettl, unpublished.
[26] G. Grüner, private communication.
[27] L. Sneddon, M.C. Cross and D.S. Fisher, Phys. Rev. Lett. 49 (1982) 292.
[28] S.N. Coppersmith and D.S. Fisher, Phys. Rev. B 28 (1983) 2566.
[29] S.N. Coppersmith, unpublished.
[30] P.E. Tua and J. Ruvalds, unpublished.
[31] S. Doniac, private communication.
[32] J.W. Brill and W. Roark, Phys. Rev. Lett. 53 (1984) 846.
[33] G. Mozurkewich, P.M. Chaikin, W.G. Clark and G. Grüner, in Charge Density Waves in Solids, Gy. Hutiray and J. Solyom, eds. (Springer, New York, 1985) p. 353.
[34] S.N. Coppersmith and C.M. Varma, Phys. Rev. B 30 (1984) 3566.
[35] J.W. Brill, W. Roark and G. Minton, unpublished.
[36] M.S. Sherwin and A. Zettl, unpublished.
[37] L. Sneddon, unpublished.
[38] A. Zettl, M. Kaiser and G. Grüner, Solid State Commun. 53 (1985) 649.
[39] M.F. Hundley and A. Zettl, Phys. Rev. B (15 Feb. 1986).
[40] S.E. Brown, A. Janossy and G. Grüner, Phys. Rev. B 31 (1985) 6869.
[41] A. Zettl and G. Grüner, Phys. Rev. B 26 (1982) 2298.
[42] H. Mutka, S. Bouffard, J. Dumas and C. Schlenker, J. Physique Lett. 45 (1985) L-729;
M.P. Everson and R.V. Coleman, unpublished.
[43] R.P. Hall, M.S. Sherwin and A. Zettl, Phys. Rev. Lett. 52 (1984) 2293.
[44] R.P. Hall and A. Zettl, Solid State Commun. 55 (1985) 307.
[45] R.P. Hall and A. Zettl, Solid State Commun. 57 (1986) 27.
[46] R.P. Hall, M.S. Sherwin and A. Zettl, Phys. Rev. B 29 (1984) 7076.
[47] R.P. Hall, M.F. Hundley and A. Zettl, unpublished.
[48] R.L. Kautz, J. Appl. Phys. 52 (1981) 6241.
[49] K. Wiesenfeld, J. Stat. Phys. 38 (1985) 1071.
[50] K. Wiesenfeld, Phys. Rev. A 32 (1985) 1744.